REPORT DOCUMENTATION PAGE

Form Approved
OMB NO. 0704-0188

1. AGENCY USE ONLY (Leave Blank)	2. REPORT DATE 07/12/2006	3. REPORT TYPE AND DATES COVERED Final, 3/1/2005-11/30/2005

4. TITLE AND SUBTITLE
Technical Report on Atomistic and Dislocation Dynamic Modeling of Plasticity in Polycrystalline Metals

5. FUNDING NUMBERS
W911NF-05-1-0088

6. AUTHOR(S)
Horacio D. Espinosa
Brian Hyde; Ravi Agrawal

7. PERFORMING ORGANIZATION NAME(S) AND ADDRESS(ES)
Northwestern University, Department of Mechanical Engineering, #B224, 2145 Sheridan Rd., Evanston, IL 60208

8. PERFORMING ORGANIZATION REPORT NUMBER OSRP Award# 31705

9. SPONSORING / MONITORING AGENCY NAME(S) AND ADDRESS(ES)

U. S. Army Research Office
P.O. Box 12211
Research Triangle Park, NC 27709-2211

10. SPONSORING / MONITORING AGENCY REPORT NUMBER
48377.1-EG-II

11. SUPPLEMENTARY NOTES
The views, opinions and/or findings contained in this report are those of the author(s) and should not be construed as an official Department of the Army position, policy or decision, unless so designated by other documentation.

12 a. DISTRIBUTION / AVAILABILITY STATEMENT
Approved for public release; distribution unlimited.

12 b. DISTRIBUTION CODE

13. ABSTRACT (Maximum 200 words)

In this effort we have studied in atomic detail the structure / property relationship of geometrically realistic metallic nanowires. It has been shown that surface roughness can greatly affect defect nucleation as nucleation from the surface dominates. Twin boundaries were introduced and were found not to be favored as sites for defect nucleation but do lead to deformation hardening as they are efficient obstacles against dislocation propagation. The details of heterogeneous dislocation nucleation have been studied in depth showing the initial state of local stress determining the strength of the defect is very complex having many sometimes competing components.

Three point bending tests performed by simulated nanoindentation experiments yield qualitative results very similar to recent atomic force microscopy investigations. Preliminary results subject to complex states of bending stress show the possible roles pressure may play in dislocation nucleation as well as propagation. Region of high hydrostatic stress appear to prohibit dislocation nucleation and propagation. Currently we are refining our simulation methods to include accurate force measurements from our simulated nanoindenter for direct comparison with current experimental efforts.

14. SUBJECT TERMS	15. NUMBER OF PAGES
Nanowires, dislocations, lattice defects, surface defects, molecular dynamics, plasticity.	34
	16. PRICE CODE

17. SECURITY CLASSIFICATION OR REPORT	18. SECURITY CLASSIFICATION ON THIS PAGE	19. SECURITY CLASSIFICATION OF ABSTRACT	20. LIMITATION OF ABSTRACT
UNCLASSIFIED	**UNCLASSIFIED**	**UNCLASSIFIED**	**UL**

NSN 7540-01-280-5500

Standard Form 298 (Rev.2-89)
Prescribed by ANSI Std. 239-18
298-102

Technical Report on Atomistic and Dislocation Dynamic Modeling of Plasticity in Polycrystalline Metals

Professor Horacio Espinosa – Priniciple Investigator
Northwestern University

(2) Table of Contents

(3) Table of Figures

(4) Statement of the Problem Studied

Metallic nanowires have become the subject of an extensive effort in recent years by the scientific community as whole. Experimental efforts have proven successful at producing large numbers of wires of varying compositions with excellent control over atomic structure. Meanwhile owing to the current difficulties with manipulation and handling of these structures, computational efforts have taken the charge exploring multiple novel aspects of structure and mechanical properties including single crystal orientations, helical structures, and single atom chains. Our goal is to study the mechanical behavior of mass producible, template synthesized wires at realistic sizes, geometries, and structures. Moreover we wish to understand how defects which are always present to some degree in real wires affect material properties. These motivations arise from the many possibilities arising for the use in microelectromechanical systems (MEMS) and microelectronics.

Background and Motivation

Nanowires are primarily formed by two distinct processes. A top down process in which ion-beam, scanning probe lithography, or electron beam is used to thin the nanowire from the bulk material is the most flexible method with regard to wire shape.[1] Nanowires formed in this manner typically are very small in size and often undergo various reorganizations once removed from the bulk in response to the high surface to volume ratio. High surface to volume ratios, and resulting high surface energies, have been shown to drive the reorientation of Au thin films from (100) to (111) when film thickness were less than eight atomic layers.[2] It has been demonstrated in Au nanobridges, cut from (100) thin films with orientation axes [001] and thicknesses smaller than 2nm, that reconstruction occurs into hexagonal prism shapes with [110] axes and {111} lateral surfaces.[3] This later was investigated specifically using atomistic simulations showing that Au nanowires with similar configuration and cross sectional areas less than 1.83 x 1.83 nm spontaneously reorganized into body-centered tetragonal (BCT) structures.[4,5] Sizes larger than these reported in either case did not exhibit any transformation.

Experimental nanowires fabricated in this way are driven to minimize their surface energy and have been observed in high resolution transmission microscopy (HRTEM) to have helical or coaxially oriented structures when further reduced below 1.5 nm widths.[6] These “weird” structures have also been investigated through atomistic simulation.[7-10] While these structures do not have optimal packing at their cores, they do have optimal surface structures.[11]

Mechanical testing of metallic nanowires is extremely limited owing to the unique challenges presented by nanomanipulation. Nanowires of short length (typically 1-5 nm) are easily formed between metals utilizing slow retraction of the contact point utilizing scanning tunneling microscopy (STM)[12,13] or atomic force microscopy (AFM).[14] These fabrication techniques generally result in single crystal structures which demonstrate

quantized plastic behavior[15-18] and asymmetric yield strengths.[14,19] During elongation of both Au nanocontacts and nanobridges it has been shown that wires transition from nanometer scales to the atomic scale via necking where they begin to fail by ideal atomic separation.[14,19-26]

Processing methods able to produce large numbers of nearly single crystal Au nanowires with high aspect ratios (length to width) utilize electrochemical replication of cylindrical pores in nonconductive porous membranes, also known as the template synthetic method.[27-30] It has been found that single crystal Au wires grow epitaxially primarily along the [111] direction with fewer than 10% showing [110], [100], and [112] orientations.[27] Primarily these wires exhibit characteristic defects such as stacking faults, twin boundaries, and a variety of surface defects or surface steps.[31]
Giving the current difficulties with manipulating nanowires on the dimensional scale of a few to tens of nanometers, there has been no experimental mechanical testing of these structures performed to the best of our knowledge.

To this point the majority of simulations have been performed in order to investigate the unique or smallest structures created by nanocontacts or top down processing, including single atom chains, helical or shell-like structures. The simulations which have been performed have been mostly aligned along [100] and have been rectangular in shape in order to investigate the effect of the higher energy [32] surfaces.[5] Some yield tests of [110] and [111] wires have been simulated at sizes smaller than 6nm.[19,33] These wires are generally defect free and always maintain simplified rectangular or rhombohedral geometries. In this work we address the considerations that must be made in order to understand nanowires typical of the bottom-up or template synthetic method. Moreover we wish to present the role common occurring defects such as surface roughness or steps and twin boundaries have on the yield stress and elastic properties.

This work also serves as support to guide our understanding for our current experimental efforts currently in progress. We have developed a novel MEMS device for the mechanical testing of nanostructures. These simulations allow for a near 1:1 size scale comparison with simulated nanostructures and real experimental

Computational Setup and Methods

All molecular dynamic (MD) simulations in this study were performed using the parallelized code LAMMPS[34] with potentials of the embedded atom method (EAM).[35] Molecular dynamics can be seen as a simulation of a system that evolves over a period of time where its particles move along their physical trajectories as determined by the equations of motion. Temperature is then accounted for by scaling the velocities of the atoms as prescribed by statistical mechanics. In the EAM framework the total energy of the system is composed of two terms. The first term describes a pair potential representing the attractive and repulsive electrostatic interaction between two atoms, i.e. a Morse potential. The second embedding energy term is based on the Hohenber-Kohn theorem which states that the energy contribution of an atom on its surrounding neighbors is a function of the local electron density due to all the surrounding atoms.[36]

This approach becomes particularly important when defects such as vacancy clusters, free surfaces, grain boundaries or dislocation cores are introduced in the material. The EAM potential for this study was determined empirically by fitting to the sublimation energy, equilibrium lattice constant, elastic constants, and vacancy formation energy for pure bulk Au.[37] Molecular statics algorithms were also employed within the same EAM framework to find zero temperature minimum energy configurations.[38]

Wires were initially created by placing atoms in positions representative of the bulk configuration in a cubic block with prescribed crystallographic orientations. Cylindrical wires were then cut from these blocks such that the initial length was set to be three times the diameter. Single crystal samples were created from 5 to 17.5nm in diameter for both [111] and [110] axial orientations. Periodicity is maintained in the direction of the wire axis at all times in order to avoid end effects while the radial directions were left to be free surfaces. Molecular statics energy minimization was then employed to find the equilibrium configuration for all wire sizes and orientations.

Figure 1A shows a [111] axially oriented virtual sample shown after relaxation. Tensile surface stresses cause the wires to contract along its length with respect to the bulk. Compressive stresses in the wire core balance the tensile surface stresses when the wire is in equilibrium.[5] Figure 1B shows a plot of equilibrium axial strain versus diameter for both orientations of wire sizes 5nm – 17.5nm. Wires oriented [110] show the greatest amount of strain with a 5nm wire achieving equilibrium at nearly 1% axial compression while [111] oriented wires of the same diameter achieve approximately half the value for the same size. Both orientations begin to have very little "intrinsic" uniaxial strain as sizes approach 20nm. The equilibrium structure was tested for assurance that a local minimum was not found by the energy minimization by annealing the nanowires using molecular dynamics. Temperature was gradually raised from 2K to 600K in 400ps held for another 400ps, and then linearly lowered back down to 2K in 400ps. The time constant for integration of the equations of motion is held as 2×10^{-15} s for all simulations in this study. No change in structure was observed between nanowires after the annealing process or after energy minimization.

Single Crystal Tensile Tests

Orientation [111]

Starting with the equilibrium configurations obtained from the energy minimization, we performed a constant number of atoms, constant volume, and constant temperature (NVT) simulation for uniaxial yield tests of nanowires up to 10% strain. Tensile tests were performed at a simulated temperature of 2K and were carried out for 10^6 time steps for a total of 2ns employing a Nose-Hoover thermostat.[39,40] This equates to a strain rate of 5×10^7 s^{-1}. Although still high when compared with experiments, this is well below the amorphization point, and is expected to contribute slightly to higher yield stresses.[41,42] To apply traction we introduce displacements on all atoms varying linearly from the center to ends of the sample in the tensile direction to avoid inducing a shock wave. For the calculation of stress we employ the virial stress method.[43,44]

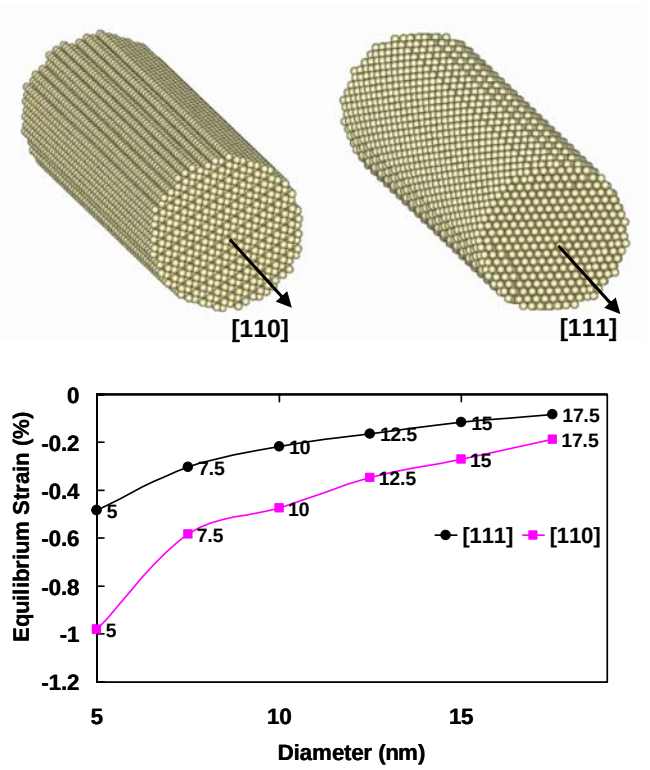

Figure 1: Top - Virtual cylindrical Au wires with two common occurring orientations. Bottom - Equilibrium axial strain as a function of diameter after relaxation due to surface stresses.

Figure 2A shows tensile stress-strain curves for wires of representative diameters between 5nm and 17.5nm, in [111] axial orientation. The Young's modulus can be fit from data using initial elastic response of the wire up to the yield point. This nonlinear elastic fit for the Young's modulus refers to the zero strain limit of the tangent modulus.[45] In the case of [111] wires the modulus does not change appreciably over the diameters studied. For this orientation the Young's modulus is calculated to be slightly above the predicted continuum theory of 116.2 GPa at all sizes studied and does exhibit some nonlinear elasticity as predicted by the potential when separations become large.[46]

Uniaxial testing revealed that yield occurs through the sudden nucleation and propagation of multiple leading partial <112> dislocations on the {111} planes originating from the surfaces. In this case these are the {112} surfaces of the nanowire owing to the presence of atomically sharp and high energy protrusions of the {111} planes. Figure 2B shows a snapshot of a 5nm [111] wire just after the initial release of the leading {111}<112> partial dislocations (~6% strain) through the visualization of stacking faults. This analysis employs the use of the centrosymmetry parameter which is a measure of the departure from pure elastic distortions in a symmetric lattice.[47] Atoms with stacking fault coordination have been exaggerated such that the defects may be more easily visualized. A few stacking faults soon disappear as the trailing partials are emitted on the same slip plane and create a perfect {111}<110> translation. This is due to the interaction of the partials within the wire, and is not generally favored owing to the fact that the uniaxial Schmidt factor is smaller for the trailing partial at this orientation.

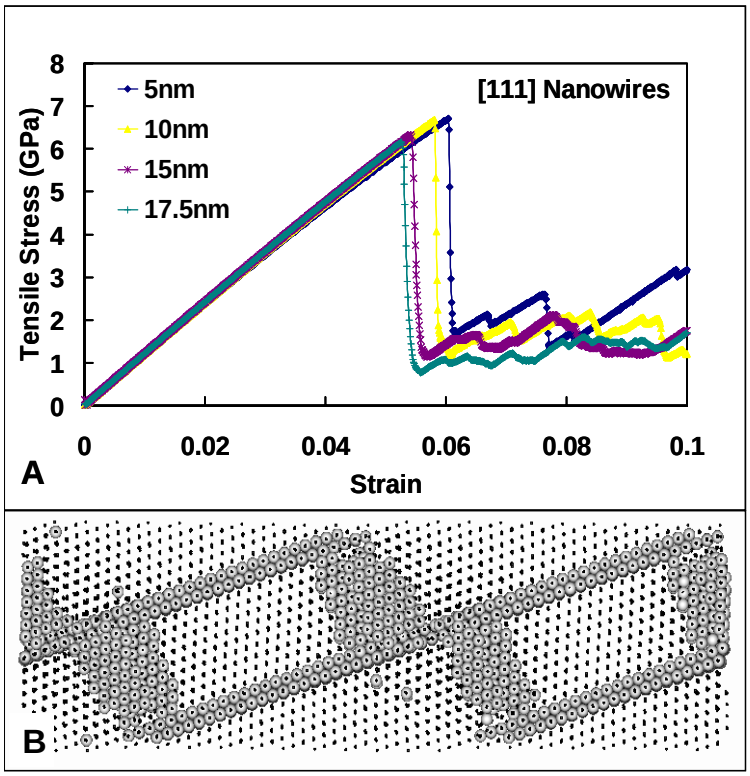

Figure 2: A) Tensile stress vs. strain curves for [111] oriented wires. B) Snapshot of 5nm [111] wire taken immediately after yielding. Exagerrated atoms are in stacking fault environment.

Orientation [110]

Figure 3A shows tensile stress-strain curves for wires of representative diameters between 5nm and 17.5nm, in [110] axial orientation. Whereas wires oriented [111] experience and elastic stiffening of the Young's modulus, an elastic softening or lowering of the Young's modulus by 4.5% traversing 5nm to 17.5nm occurs. Again, both orientations do exhibit some nonlinear elasticity as predicted by the atomic potential when separations become large therefore the modulus is incorrectly calculated if this is not taken into account. Nanowires oriented [110] initially are above the theoretical value of 80.9 GPa but drop slightly below this value as thickness increases above 12.5nm.

The first large drop in load carrying capacity in the [110] wire occurs in the rapid emission of leading {111}<112> partial dislocations. Initially there are 2 partials emitted from the high energy {100} surface of the wire which rapidly travel to the opposite side. One of these partials upon reaching the opposite surface triggers the release of a third {111}<112> partial from the defected surface. One trailing partial is seen to be emitted, but once again it is not without the interaction of another defect, in this case a stacking fault. Figure 3B shows a snap shot of a [110] Au nanowire at 8% strain after the initial stress drop has occurred. From this figure the primary mechanism of plasticity for [110]

wires is clearly illustrated. Leading partials are consistently emitted on adjacent {111} planes causing necking and the creation of twin boundaries.

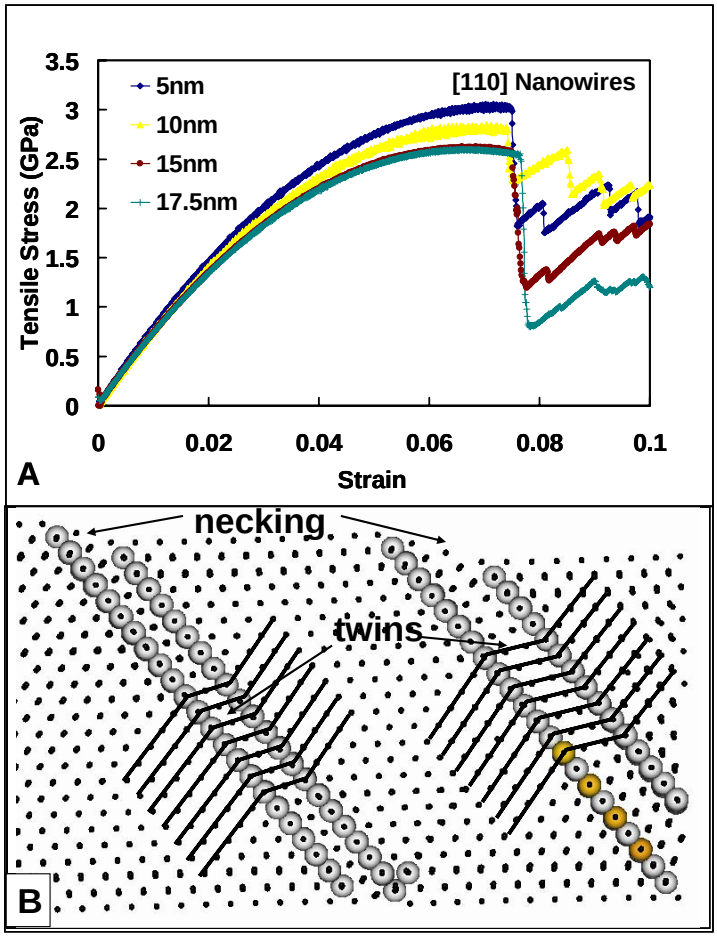

Figure 3. A) Tensile stress vs. strain curves for [110] oriented wires. B) Snapshot of 5nm [110] wire taken immediately after yielding. Exagerrated atoms are in stacking fault environment.

The Effects of Temperature

In order to understand the effects of temperature on the yielding behavior, tensile tests were performed at simulated temperatures ranging from 2K to 600K. Five nanometer diameter wires were equilibrated using a constant number, pressure, temperature thermodynamic ensemble, or NPT, at each temperature investigated. This computational setup was used such that the entire sample may find its equilibrium configuration, including equilibrium atomic spacing, at the desired temperature. These equilibrated structures were then used as before for uniaxial tensile tests in the NVT ensemble.

Figure 4A shows a plot of the yield stress versus temperature for the 5nm diameter wires. The yield stress was seen to decrease significantly with increasing temperature with a 45% decrease at 300 K° and 55% decrease at 600 K°. The decrease in critical yield stress is not due to a change in the mechanism. As for all cases the wires yield as previously explained; (111) <112> type partial dislocations generated from the free surfaces.

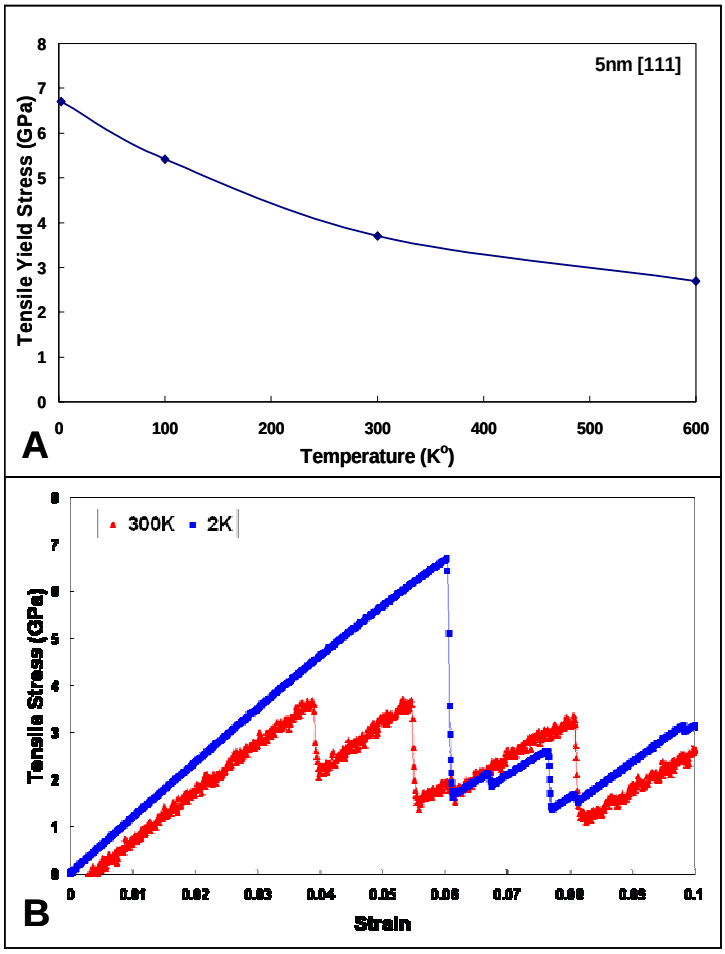

Figure 4 A) Tensile yield stress as a function of increasing temerpature. B) Tensile stress vs. strain for 2K and 300K temperatures.

Figure 4B shows the generated stress – strain curves for the 2K and 300K cases. From this plot one can see that there is a not only a significant effect in the onset of yield, but also a significant difference in the drop in load carrying capacity between the two cases. However note that the flow stress after yield becomes quite consistent between the two cases. These things will be discussed further in a later section.

Strain Rate

Molecular dynamics for all of its many virtues has the distinct drawback of only being able to access very short time scales. This leads to very high strain rates in order to apply a reasonable amount of deformation within the limits of current computational resources. This leads to overdriving of the system such that the materials may reach unrealistically high levels of stress and strain before activation of deformation mechanisms can occur.

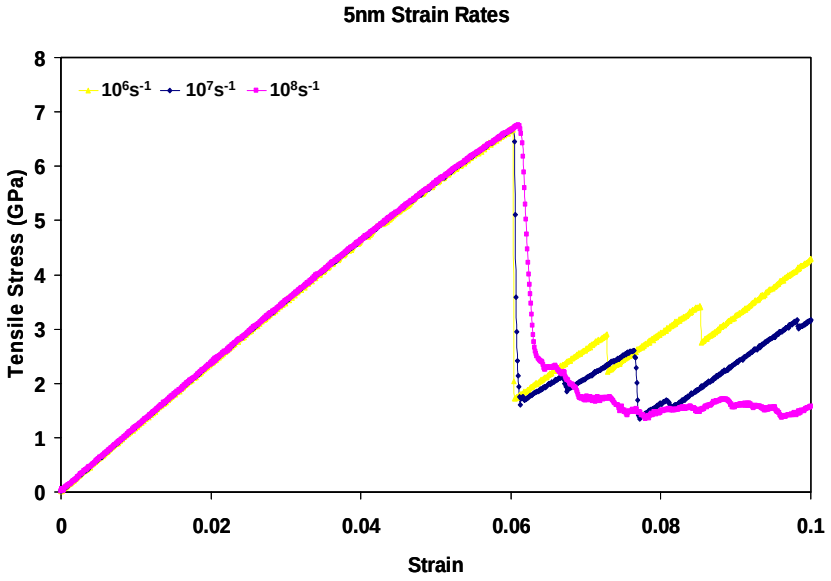

Figure 5 Tensile stress versus strain for three order of magnitude of strain rates.

To check how sensitive our simulations were to strain rates accessible to molecular dynamics we studied three orders of magnitude of strain rate. One order higher and one order lower than that of what we used for this our study. Figure 5 shows plots of the tensile stress versus strain for the 5nm diameter nanowire at three strain rates 10^6 s^{-1}, 10^7 s^{-1}, and 10^8 s^{-1}. For these strain rates we observe almost no difference in initial stress levels at the yield point with the faster rates edging subtly higher. However, the resulting flow stress behaves quite differently. At the highest strain rate the system is being overdriven such that nucleation is occurring simultaneously with propagation throughout the length of the wires. Likewise many more dislocations have been emitted at the onset of yield with very little time for equilibration before more dislocations are emitted from the surfaces. Often trailing partials are emitted almost instantly after the leading owing to the rapid loading of the system.

For the two slower rates, qualitatively the process proceeds in the same way. It appears that the only difference between the two slower cases has to do with the statistical nature of the nucleation. Emission occurs at different random points on the free surface resulting in different interactions during loading. Phenomenologically these

processes are the same eventually resulting in very similar overall flow behavior. This adds merit to our choice of $10^7 s^{-1}$ such that we are able to access much longer times without the loss of meaningful information.

Twin Boundaries

The most frequent structural defect other than general surface roughness or other surface defects is the presence of twin boundaries. In deposited Au nanowires of [111] orientation twin boundaries appearing perpendicular to the growth axis of the type $(111)[11\bar{2}]$ and are considered the primary twin; see Figure 6A. No twinning or stacking faults have been observed in nanowires grown along the [110] orientation.[31] Virtual samples were created with identical dimensions used previously for the study of perfect wires with one primary $(111)[11\bar{2}]$ twin located at the center of the wire; Figure 6B. As in the case of the surface step, periodicity causes another twin boundary to exist at the ends of the wire. This results in the "bamboolike" crystalline structure that has been reported to be controlled by careful manipulation of the electrodeposition parameters.[48] The effects of this configuration will be addressed specifically in the next section.

Uniaxial tensile tests were performed using the same parameters as discussed previously for comparison and tensile stress-strain curves were produced from the data. Performing the nonlinear elastic fit to the stress-strain response up to the onset of yield revealed no significant change in Young's modulus for all sizes tested as compared with wires without the twin defect. Tensile yield strength however was affected by the presence of the twin boundary. The stress required for the nucleation of the dislocations was observed to be 18-22% less than that of the perfect wire with corresponding diameter, with the smaller diameters being slightly more affected.

The twin boundaries themselves were not sources for the nucleation of the dislocations, but rather the surface disturbed near the boundary. Figure 7 helps give a closer view of what the surface and boundary looks like. Boundary atoms or mirror plane of the twin boundary have been exaggerated for easy recognition. The atoms near the boundary that are also exaggerated are the first atoms to begin to have non-zero centrosymmetry during the tensile test and do so before any nucleation event occurs. This is due to the fact that the atoms above are in a state of high tensile stress resulting from the {111} faceting observed in this orientation.[48] This role of the {111} facets is characteristic of all the nucleation events in [111] nanowires however the presence of the twin has slightly changed the local stress state causing heterogeneous nucleation rather than the eventual nucleation from thermal fluctuations. The six-fold symmetry of the orientation causes the faceting, however only 3 of the 6 facets appearing are sites for nucleation owing to the orientation of the twin. This can be seen by the slightly different local environment of the facet located at the top of the Figure 7 as compared with the bottom facet which is almost homogenous with the other facets in the region of the twin.

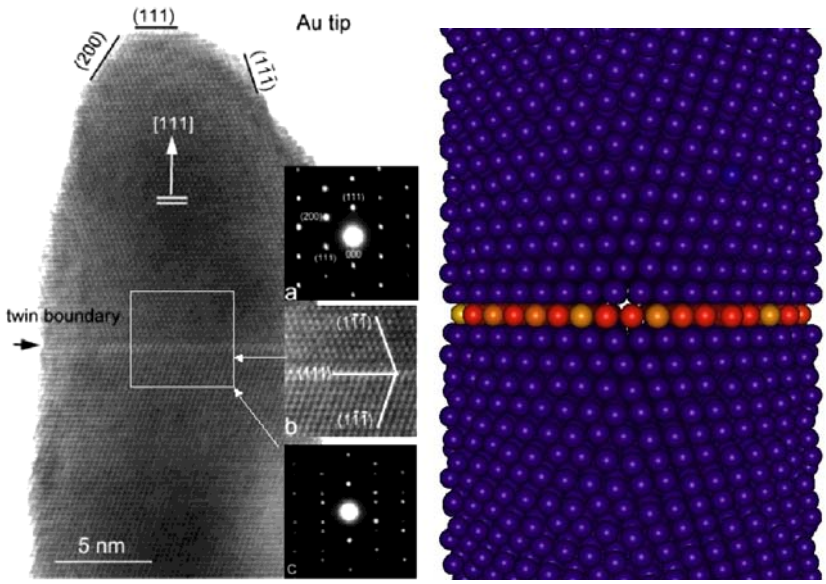

Figure 6 A) TEM image of primary twin boundary oriented perpenticualr to wire axis [111]. B) Corresponding virtual sample; cylindrical with prmary twin boundary shown.

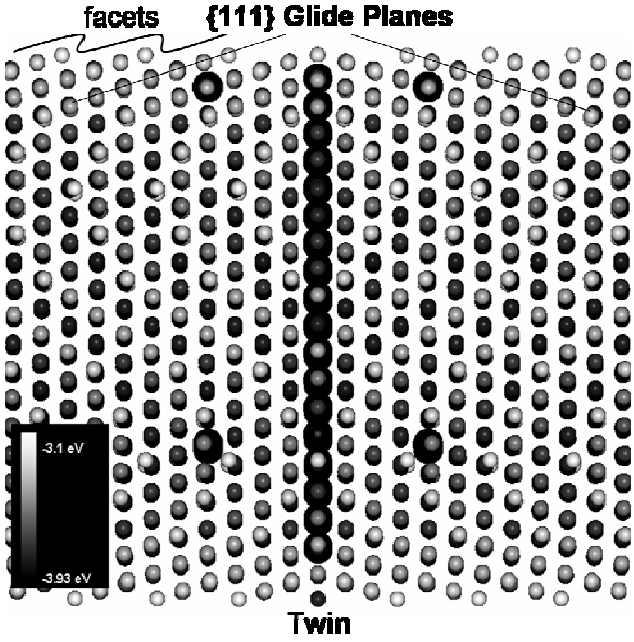

Figure 7 A twin boundary present in center of [111] oreirnted nanowires. Lighter atoms are of higher energy. Dislocations are nucleated from surfaces defected by twin boundary.

At higher levels of strain we observe that the twin boundaries do begin to emit embryonic dislocation loops, however these dislocations are never seen to be emitted as the surfaces emit first relieving the associated stress; see Figure 8. The twin boundaries

appear to be very effective obstacles against the propagation of the dislocations and dislocations begin to pile-up are the boundaries. This does lead to some observed hardening suggesting that twins may not be altogether unfavorable especially in the presence of surface roughness.

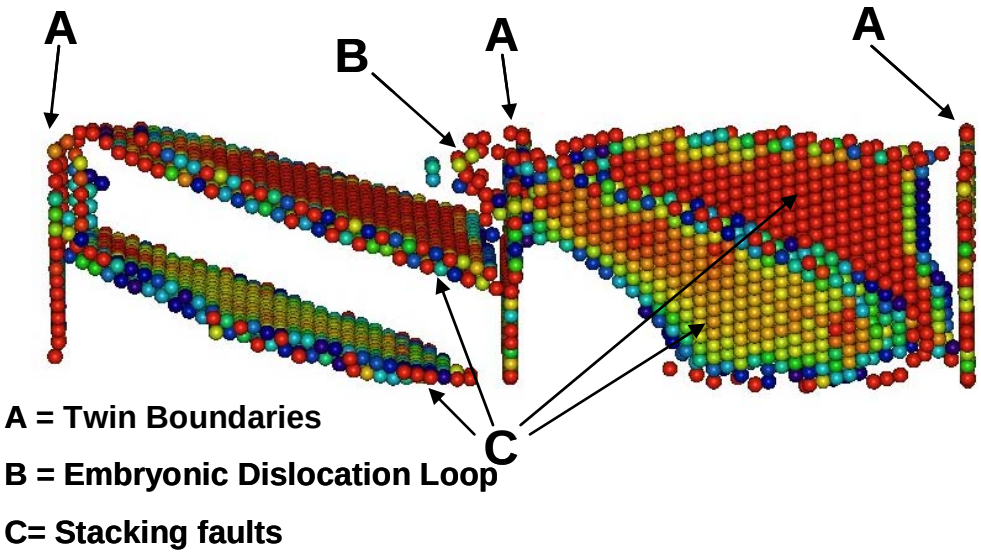

Figure 8 Snapshot of nanowire taken just after the onset of yield. Only atoms in local stacking fault or dislocation environments are shown. Dislocation loop emanating from the boundary is seen but was not observed to be favored over further surface nucleation.

Bamboo

From our initial investigation of the effects of twin boundaries present in the [111] oriented nanowires, we have found a number of interesting effects. First, the twin boundary itself is not a dislocation sources, but rather it is the disturbance which it causes in the otherwise "perfect" surface from which they emit. Secondly we have seen some evidence of hardening from the stress – strain relationship as well owing to the fact that the twin boundaries are efficient obstacles to the propagation of the dislocations.

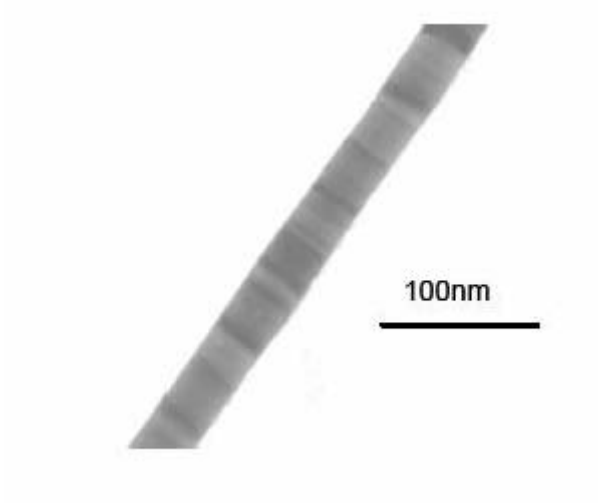

Figure 9 TEM image of gold nanowire exhibiting "bamboo" structure. This structure is created by the formation of periodic twin boundaries perpendicular to the wire axis.

Figure 9 is a TEM image taken from the work of Wu and coworkers showing a typical "bamboo" structured wire[49]. These it has been shown that these structures can be controlled by careful manipulation of the deposition parameters. Furthermore in the interest of nanoelectronics twin boundaries are known not to significantly affect conductance. This makes this unique structure interesting since it could be an avenue of strengthening for application that might experience load.

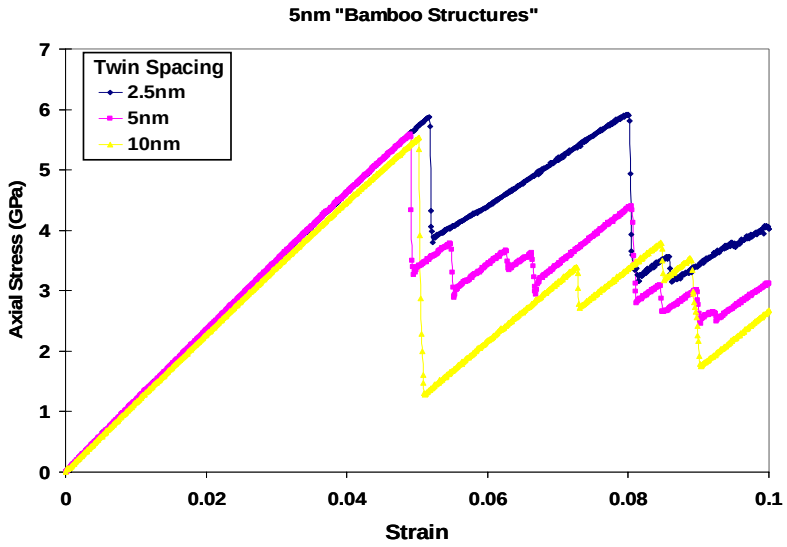

Figure 10 Axial stress as a function of strain for three twin boundary spacings in 5nm diamter "bamboo" structured wires

To investigate the effect of these periodic twin boundaries we created three 5nm wires in which we varied the spacing between the twin boundaries. These samples were created such that the periodicity created the bamboo structure. Wires were created with up to 5 physical twin boundaries present before utilizing periodicity but showed no difference in results.

As seen in Figure 10, initially and elastically these three cases respond almost identically. Yielding also occurs nearly at the same stress level. The dislocations are of the same character and type as discussed for the twin in the previous section with nucleation still only occurring at the free surfaces. However the response after the onset of initial yielding appears to be quite different. Most obvious is the difference in the initial drop in stress level. This owes to the fact that dislocations propagate further with larger spacing relieving more stress.

Secondly and more importantly we begin to see a large increase in the hardening rate as the twin spacing decreases. Again this is due to the fact that the twin boundaries are obstacles to the propagation of dislocations and as such are pinned forcing the stress to increase to a higher level to either generate the trailing partial and alleviate the stacking fault, or nucleate elsewhere along the surface. This as such again leads to more networking and pinning of dislocations. This shows that hardening can be improved in this manner.

Surface Defects

A Surface Step Model

Although very near to single crystal in structure, real nanowires fabricated via deposition techniques are never truly defect free owing in part to the fact that the surface of the pores of the template are never atomically flat. As a first step understanding the role of surface defects we have created virtual nanowires with a step character. For this we have chosen the axial orientation [111] and applied a simple translation of magnitude and direction <110> along the (111) plane aligned perpendicular to the wire axis; see Figure 11A. This was done such the translation is equivalent to a perfect dislocation of the fcc lattice and therefore does not introduce a stacking fault. Energy minimization was then implemented to allow the defects to equilibrate to their lowest energy configuration. Molecular dynamics was also employed in the annealing scheme previously discussed and no change in structure was observed when compared with the results of the molecular static relaxation.

Tensile tests up to 10% strain were performed under the same boundary conditions and strain rate implemented for defect free single crystal wires. Tensile stress-strain curves were generated for sizes between 5 and 10nm. First a comparison with perfect wires was made to check the influence on Young's modulus of the step defect. The 5nm diameter nanowires experienced a 4% decrease in modulus, whereas in the 10nm thickness the effect was smaller with only a 2.5% decrease.

Yield stress and stress-strain response of the defected wires however showed a much more significant impact. Figure 11B shows representative tensile stress-strain

curves of the 5nm wires with and without the presence of a surface step. At 5nm thickness the tensile yield stress shows a significant decrease of approximately 30% with the step defect. The effect of the step as the diameter of the wire increases also increases. At 7.5nm the decrease is 38% and at 10nm the effect is more pronounced showing a 50% decrease in yield stress.

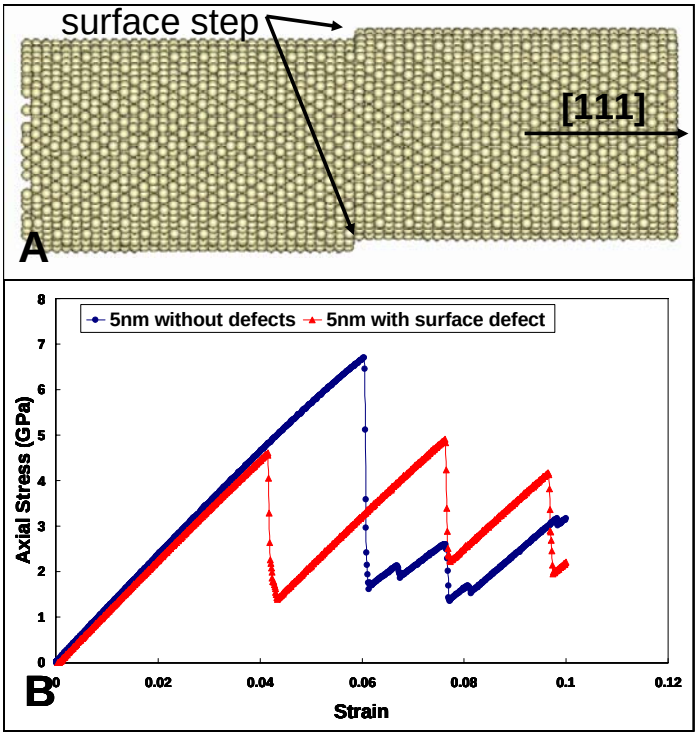

Figure 11 A) Simulated gold nanwire with 1/2 [110] translation producing surface step. B) Tensile stress versus strain for 5nm diamter wires with and without surface step.

Upon inspection of the responsible deformation mechanisms we find that the nanowires with the translational step also yield by the nucleation and propagation of {111}<112> type partial dislocations. In this case however we do not see the large number of dislocations nucleated along the surfaces of the wires as we did in the perfect wires. The steps being of higher energy and stress become the sites for dislocation nucleation. For the periodic lengths tested we observe 2 partial {111}<112> type dislocations emitted, one from the step places in the middle of the sample, and one from the corresponding step created from the periodic image.

Realistic Surface Defects

In an effort to study more realistic defects in the surface morphology of metallic nanowires we have generated virtual nanowires with surface defects created by an energetic criterion. Using 5nm diameter [111] axially oriented nanowires we have selectively removed the highest energy atom(s) within a small region. The impetus of this was to simulate the way in which atoms would be selectively removed in natural methods such as chemical etching or particle bombardment where high energetics facilitate removal.

Figure 12 shows an edge view of the [111] oriented wires with facets of the {111} planes clearly visible. The highest energy atom by far is the single atom located at the top of the {111} facets. This is marked as 1 in the figure and its removal becomes our first defect case D1. After removal of the first atom the system was allowed to equilibrate for 400ps allowing time for the new structure reach its lowest energy configuration. This was done iteratively for each case such that the next atom(s) were chosen from the new equilibrated structure. Subsequently there are two atoms of nearly identical energy labeled with a 2, two more labeled with a 3 and one labeled with a 4. The additional removal of each of these represents our four defect configurations referred to as cases D1-D4.

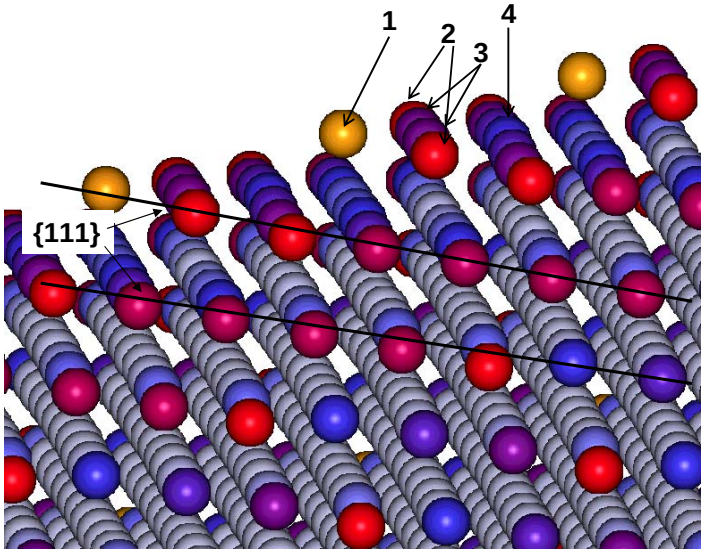

Figure 12 Image taken from side of 5nm virtual nanowire showing {111} planes and facets. Numbers indicated the successive removal of highest energy atoms.

After the selective removal of atoms each wire with its unique surface defect configuration was then tensile tested as discussed in the previous sections. Tensile tests showed a decrease in yield stress for all cases tested, albeit in the case of D1 the drop was nearly insignificant. Likewise for all cases the surface defect acted as a nucleation site for dislocation emission except for the D1 case which was not a favored location. The dislocations emitted were of the same character as in the other cases for this orientation, namely {111}<112>. Figure 13 shows the crystallographic orientation of the wire, the slip plane which yield occurs upon, and the plane normal direction.

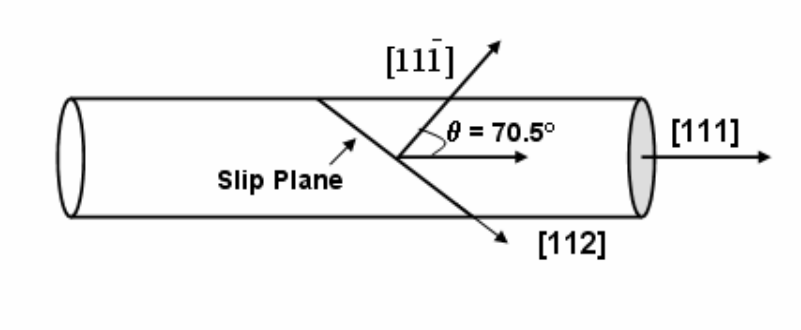

Figure 13 Schematic representation of [111] oriented nanowires showing slip plane and tensile direction [111] and angle between.

In order to better predict how the nature of a defect may affect yielding we have analyzed the various components of the stress using the virial method. Starting from the point in which we selectively remove the atoms to create the defect we take a representative volume defined by the cut-off of the atomic potential. We then construct the stress tensor representative of this volume's elements (atoms). This information we have available at any instance of time during the simulation.

In order for this information to be meaningful we first rotate our stress tensor such that 2 of diagonal elements are lie within the plane and one aligned with the plane normal. From our initial coordinate system this is a rotation of 70.5° about the z-axis such that the diagonal element originally defined by the tensile direction becomes the direction perpendicular to the slip plane. Correspondingly the remaining diagonal is rotated into the direction of slip within the plane. Figure 14 shows a schematic of the original stress components and the subsequent orientations after rotation denoted with a prime. This then creates the off diagonal component S'_{xy} meaningful such as it equivalent to the shear stress in the slip plane.

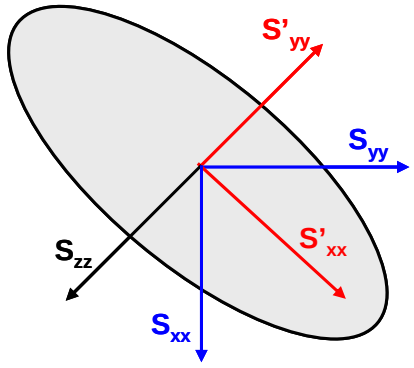

Figure 14 Schematic showing rotation of stress tensor from intial coordinate system to slip plane normal.

With all of the components of stress oriented with respect to the slip plane and the direction of slip we have analyzed the state of stress both during equilibrium and under loading. Table 1 summarizes the results of these calculations from the transformed stress tensor's shear and pressure components. From this we noted the initial condition of shear stress in the volume as well as at yield, and also the initial and yield pressures. Taking the difference between the shear stress level at which yield occurs and the initial level of shear stress present with the defect one should be able to make some predictions as to how much the defect will affect yield.

Table 1 - Resolved shear stresses and pressure both intial and at yield. These stresses are resolved from a representive volume around the introduced defect. All values are in units of GPa.

Case	S_{xy}' (ε_{yield})	$S_{xy}'_{(\varepsilon=0)}$	$S_{xy}'_{(yield)} - S_{xy}'_{\varepsilon=0}$	$S_{yy}'_{(\varepsilon=0)}$	P ($\varepsilon = 0$)	P (ε_{yield})	σ_{yield}
D1	-1.73	0	-1.73	1.17	0.7732	2.74	6.65
D2	-1.35	0.09	-1.44	1.68	1.045	3.01	5.4
D3	-1.8	0.176	-1.976	2.16	1.294	3.18	6.2
D4	-1.36	0.098	-1.458	1.83	1.137	3.07	4.7

This difference follows a trend for our four cases studied (five given the perfect case) except for the anomaly which occurs with defect case D3. Generally the strength of the defect can be seen such that

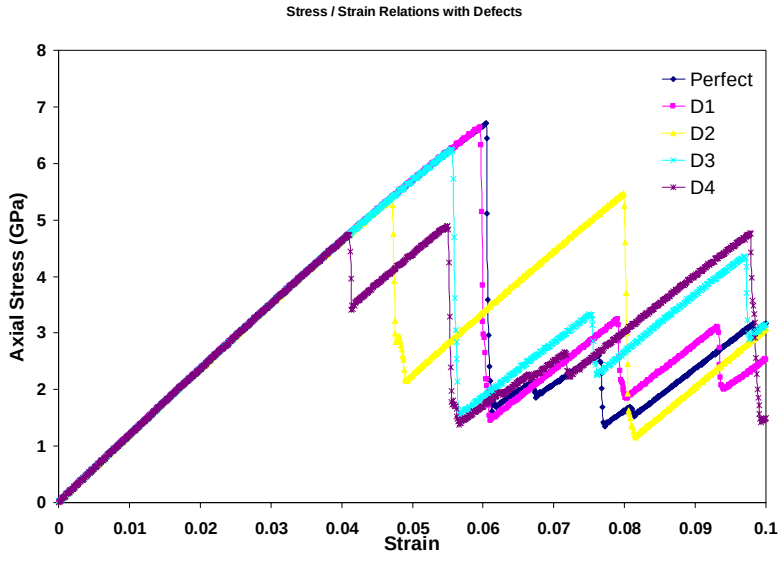

Figure 15 - Axial stress versus strain for the four unique surface defects seen in Figure 12.

Bending

As part of our ongoing effort to completely understand the elastic and plastic behavior of metallic nanowires we have begun to investigate how they respond to a bending state of stress. For this study we have implemented to cases. First, a pure bending case with one end fixed. Second, a three point bending case with both ends fixed and the force applied in the center. This latter case represents a complex state of stress with both bending and tensile stresses. These forces are applied with a simulated nanoindenter implemented in LAMMPS and modified by our group.

A gold nanowire of 2.5nm diameter and approximately 25.0nm length (aspect ratio 1:10) is modeled using LAMMPS. The axis of the wire is oriented along [111] crystallographic direction, which is aligned with y-axis of the coordinate system. The indenter is cylindrical in shape and extends infinitely along the z-axis. The cylinder is moved in x-direction at a specified speed to deform the wire. The following figure shows a schematic drawing of the model and the actual model. Origin of the coordinate system coincides with the center of the wire, as shown in the actual model. Note that in the actual model, the indenter is not physically but mathematically modeled to generate a force field to deform the wire.

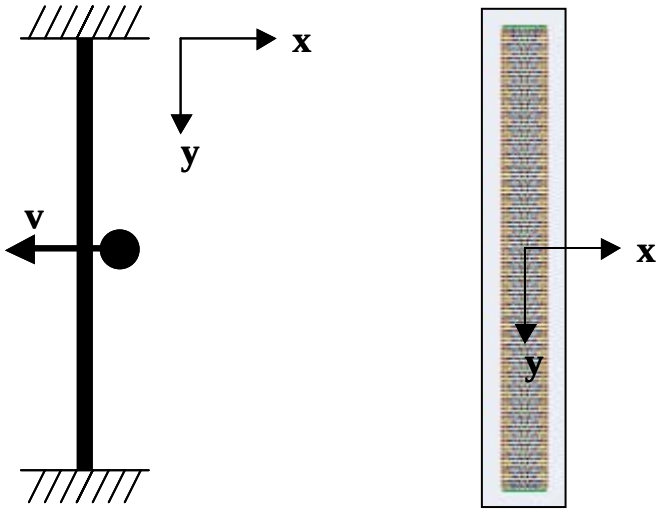

Figure 16 - A) Schematic model of the wire and indenter. B) Actual model of the wire, showing the location of origin of the coordinate system.

To clamp the two ends of the wire, four layers of atoms on each side have been set to have a zero force throughout the MD simulation. The radius of the indenter used for deforming the wire is same as the radius of the wire, i.e. around 12.0nm. The indenter repels all atoms if touches, so it can be used to push into a block of material or as an obstacle in a flow. For each time step, the coordinates of atoms lying close to the indenter are checked and all the atoms whose center lie within the periphery of the indenter see a force from the indenter based on following equation:

$$F(r) = -k\,(R-r) \text{ for } r < R$$

where *k* is the specified force constant, *r* is the distance from the atom to the center of the indenter, and *R* is the radius of the indenter. The force is repulsive and F(r) = 0 for *r* > *R*. The center of the indenter moves during the simulation, based on its initial position and the specified velocity.

The orientation of atoms along the axis of deformation i.e. x-axis is <1-10>, and the orientation along the z-axis (going into the plane of paper) is <11-2>. The indenter moves at a speed of 0.0625 Angstroms/ps along –x direction. The time step set for the simulation is 2fs, which means that the indenter moves a distance of 25.0fm (~$6x10^{-5}$ times the lattice constant) in each time step. The following figure shows the corresponding deformation patterns at different time steps. It can be observed that wire sees some plastic deformation at t = 360ps, which corresponds to a deformation of around 22.5 Angstroms at the center of the wire.

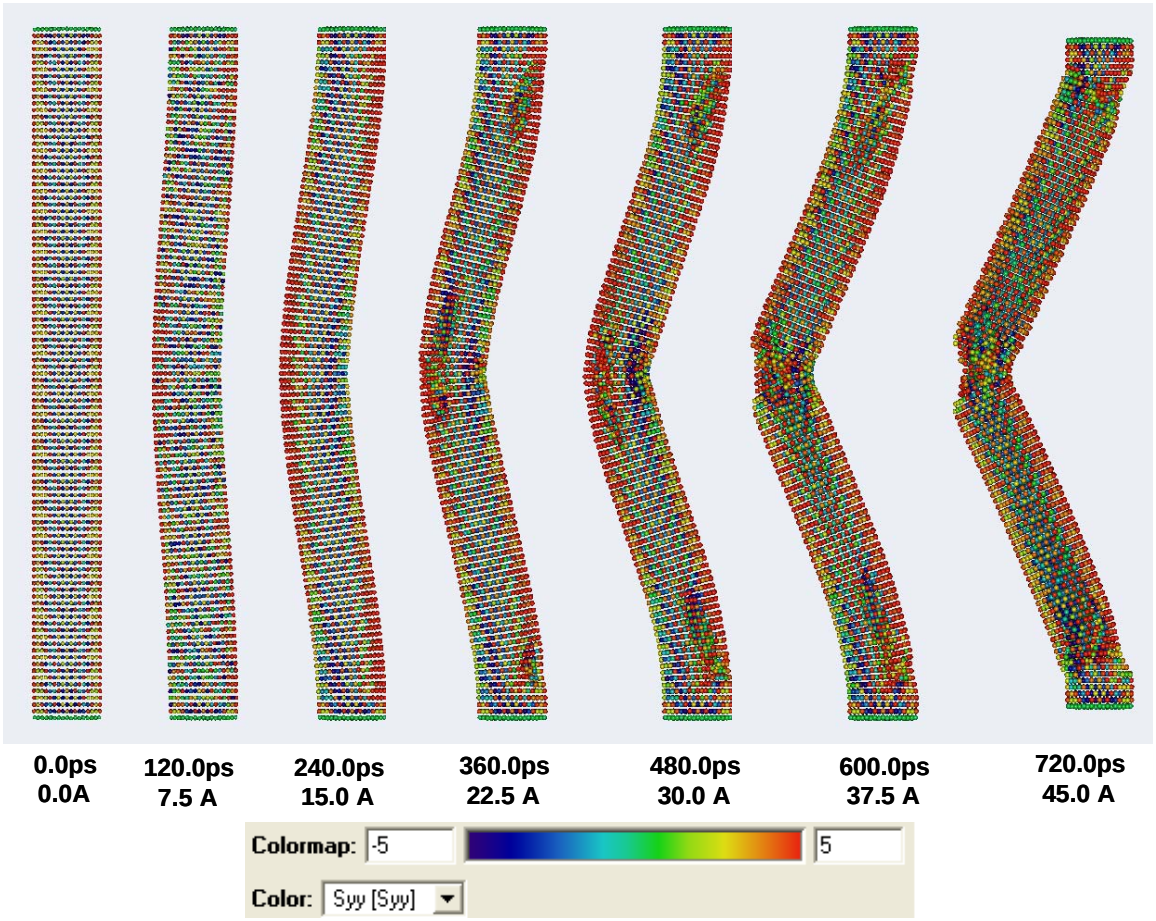

Figure 17 - Deformation pattern of the wire at different time steps. The longitudinal stress (Syy) has been plotted here. The values shown are the time and deformation at center at that time.

Strain rates are calculated based on beam theory of continuum mechanics. In the model described above, there are two deforming mechanisms involved. The bending of the wire,

which is more prominent at the ends than at the center and the tension induced in the wire at large deformations. The maximum strain rate due to the bending can be approximated by the following expression:

$$(d\varepsilon/dt)_{bending} = 6dv/L^2,$$

where d is the diameter of the wire, v is the speed of the indenter and L is the free-standing length of the wire. On the contrary, the maximum strain rate due to tension does not depend on the diameter but the deformation at the center. It can be expressed as:

$$(d\varepsilon/dt)_{tension} = 4\delta v/L^2,$$

where **δ** is the deformation at the center of the wire.

Note that the strain rate due to tension is not a constant for a given speed of the indenter but increases as the deformation increases. Moreover, the different layers of atoms along the axis of wire see different strain rates due to bending but a constant strain rate due to tension at any given point of time. The strain rates calculated using these formulas are of the order of $10^8 s^{-1}$ for bending and around $10^7 s^{-1}$ for tensile load.

The stress values at the center of the wire, as these planes are more or less perpendicular to the y-axis, have been used to calculate the normal force on the wire. We can calculate the force by multiplying these values with the cross-sectional area of the wire. As a result, the following P-delta curve is obtained:

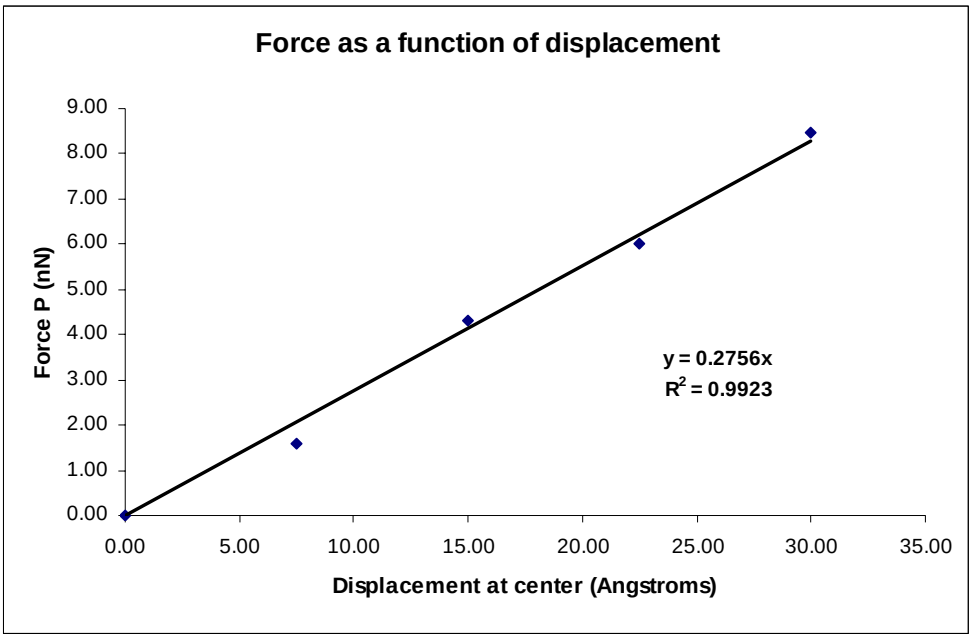

Figure 18 - Force applied by the indenter as the deformation increases. Force values shown here are calculated using the shear stress values plotted in Figure 3.

A given load is related to the deformation for the case of bending by following expression:

$$P = (192EI)(d/L^3)$$

,where E is the Young's modulus, I (=pi*r*r/4) is the moment of inertia, d is the deformation and L is the length of the wire. Using this expression, we can calculate

Young's modulus for the nanowire at different deformations. Ideally, P-delta curve should be non-linear and the value of Young's modulus should be constant for a given material in the low deformation elastic regime. However, if we calculate Young's modulus using the above stated values, the value for E does not turn out to be a constant? This might be due to the reason that the force values calculated above correspond to the shear stress only at the center of the wire. These force values are not actually the total force applied by the indenter on the wire.

Table 2 – Young's Modulus calculated from the applied load using the deformation at a given point of time. Deformation (d) is in Angstroms, Load (P) in nanonewtons and Young' Modulus in GPa.

d (A)	P (nN)	E (GPa)
0.00	0.00	-
7.50	1.57	45.47
15.00	4.31	62.46
22.50	6.00	57.98
30.00	8.45	61.22

The wire sees nucleation of defects at 360ps which corresponds to a deformation of 22.5 Angstroms at the center of the wire. The nucleation occurs at three regions as shown in the figure below. However, to precisely capture the location where it starts first, it is required to write the stress data more frequently at many time steps. It has been observed that stacking faults are developed in the high stress region due to bending. However, the stacking faults are unable to flow through the other side of the wire due to compressive stresses on the other side. Figure 19 shows the nucleating defects in three highly stressed regions of the wires. The top has been zoomed to focus on the stacking fault created in that region. Due to the circular cross section of the wire, we can also observe some skew ness in the alignment of atoms along z-axis.

A similar model for a thicker wire of 5nm diameter was also built and analyzed. Figure 20 shows the deformation profile of the wire when it starts thinning in the center, due to high tensile forces. The picture qualitatively matches with the experimental results obtained by Wu et. al. However, we observed that the atoms in the deformed region show some amorphous behavior. This can be attributed to the high strain rates which have been used for these cases. Some more analysis need to be done with appropriate strain rates of no more than 10^6 s^{-1}, so that the actual nucleation of defects and the onset of plasticity can be observed and characterized well.

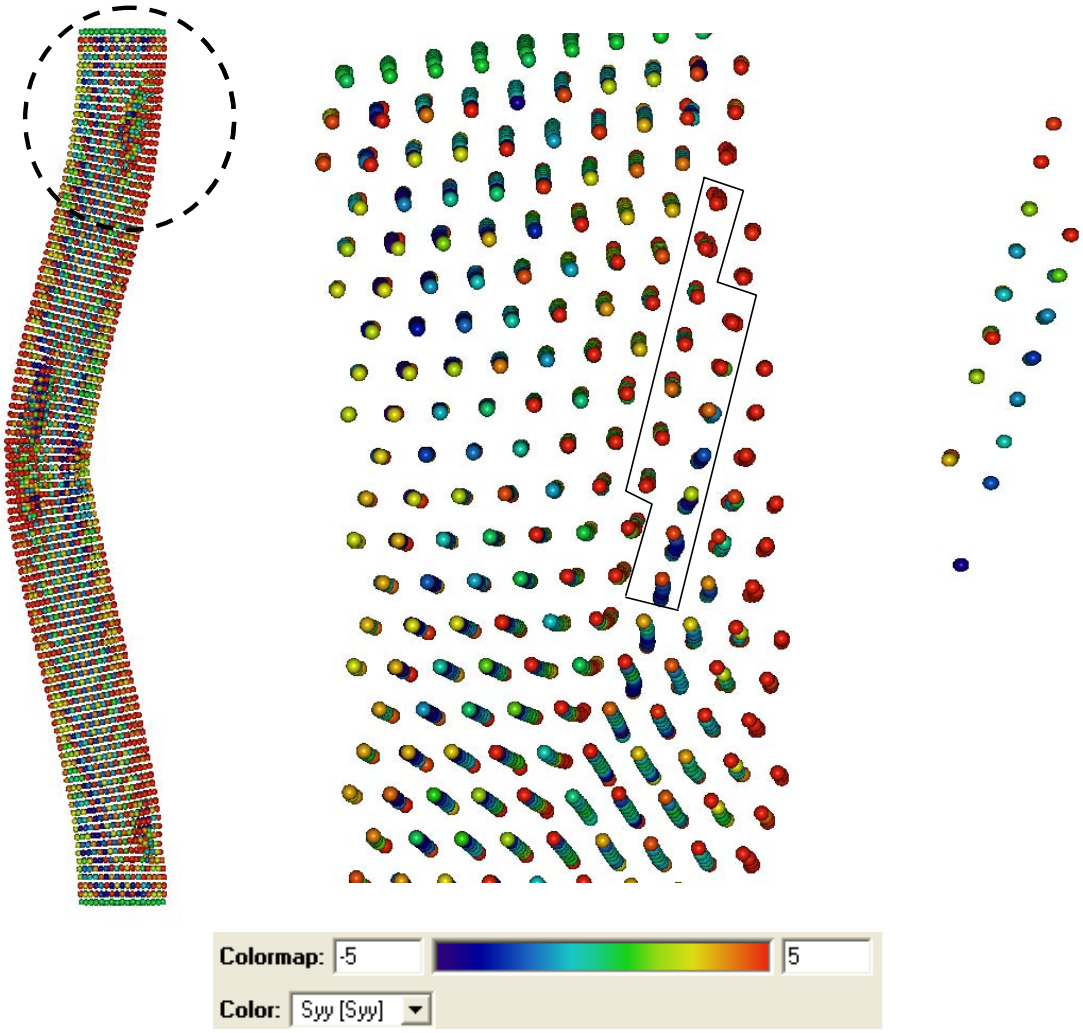

Figure 19 - A) Overall image of nanowire under deformation from 3 point bend test showing longitudinal stress. B) Enlarged image of area cirlced in part A with atoms marked which are in stacking fault local environment. C) Atoms in the stacking fault environment

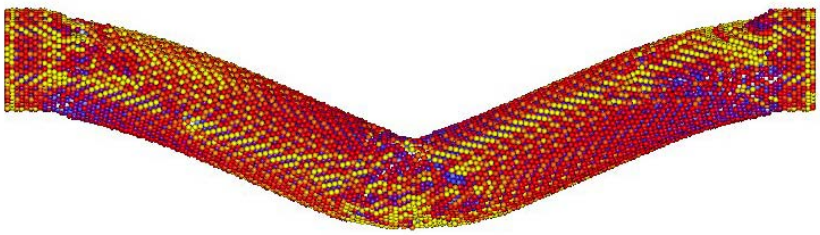

Figure 20 - Image of nanowire (5 nm diameter) under deformation from 3 point bend test. The plastic deformation at the ends of the wire and in the center can be observed.

(5) Summary of Important Results

In this effort we have studied in atomic detail the structure / property relationship of geometrically realistic metallic nanowires. Using cylindrical model wires we have looked at not only atomically "perfect" wires of various diameters, but we have also introduced and studied the effects of a number of structural defects commonly found in electrodeposited wires. Furthermore we have also looked at the effects of strain rate and temperature on the yield behavior during tensile loading.

Defect free nanowires behave similarly to that of less realistic structures reported recently in the literature. Decreasing wire diameter drives higher equilibrium strain with no applied load. This leads to an increase in yield strength that parallels the initial strained condition of wires as it opposes the tensile stress during loading. Yield mechanisms are consistent such that leading partial <112> dislocations travel on the {111} planes are always generated at the surface of the wires. Wires exhibit a catastrophic initial drop in load carrying capacity characterized by the simultaneous nucleation of multiple dislocations.

This high number of simultaneously generated dislocations is affected by a number of things. Stress can be localized by the presence of defects. In the case of surface steps or surface roughness it is equivalent to the pair (due to periodicity) or a point defect respectively. Likewise in the case of a twin boundary we have learned that the boundary itself is not a source for dislocation nucleation but rather it merely disturbs the surface such that it creates symmetric nucleation sites near the boundary. In this latter case we have multiple sites of equal strength and in the absence of high thermal fluctuations, each tend to nucleate nearly at the same time.

Taking into account the effects of temperature a picture begins to emerge where the simulation results reported to date are not entirely realistic. Real metallic nanowires will have many sources for the nucleation of dislocations owing to the surface roughness alone as well as the obvious affects of higher temperatures. Typically atomistic simulations are performed at 2K° (or similar) which provide very little random thermal fluctuations in the material. In the case of a perfectly symmetric nanowire, all of the nucleation sites are of equal strength, and thus in the absence of fluctuations and the presence of the high over driven strain rate, many dislocations are nucleated simultaneously. When a defect is present there is a local stress concentration such that yield occurs much sooner. This is further demonstrated by the twin boundary in which multiple dislocations are emitted, but only from the few symmetric sources that are of equal strength and are thereby over driven and nucleated simultaneously. Likewise this is demonstrated in the presence of higher temperatures where the increased thermal velocities increase the likelihood of the local stress concentration exceeding the critical level resulting in yield.

Many of the crystalline features of metallic nanowires such as whether they contain a single crystal orientation or polycrystalline, as well as twin boundaries can be controlled by careful manipulation of the deposition variables. However real nanowires are unlikely to ever be atomically smooth on the surfaces and therefore will always contain dislocation sources of varying strength. It seems important to note that when it comes to atomistic simulation of these structures that the onset of plasticity may not be a realistic indicator of the strength of the material. In fact it appears that the average flow

stress may be more of a consistent indicator as this seems to be fairly consistent after the onset of initial. This is reasonable as at this point the surface has been disturbed typically in multiple somewhat random locations resulting in the creation of multiple surface defects usually of different intensities.

Our in depth analysis of the local stress environment in the vicinity of the defect also has begun to shed light on the details governing defect nucleation. From our recent calculations we have shown that not only does the nucleation depend on how the defect biases the shear stress, but also how the defect affects the local stress on the slip plane affecting yield.

Our work thus far addressing bending stress is showing some interesting results. We are able to see multiple mechanisms of yielding occurring due to the complex stress state applied. Also we have observed how the compressed regions of the wires do not emit dislocations and in fact these regions do not allow dislocations to exist (up to strains tested). This observation leaves multiple questions yet to be answered on the exact role of pressure in dislocation processes.

Future Work and Direction

We have tested wires in a realistic cylindrical geometry and have found that like the rectangular approximations done by others they suffer from a perfectly symmetric constraint with respect to the loading direction. Regarding the nucleation of dislocations in single crystal type metallic nanowires we have shown the importance of including defects, in particular surface defects, in the model. Form this work we have observed both in the bending tests as well as in our defect studies the role of hydrostatic stress in dislocation mechanisms. For this we are performing many more calculations to better understand precisely what these roles are. To this end we may then make suggestions such that these devices may be improved by systematically avoiding or removing certain defects.

The three point and pure bending tests are quite new results and need further refinement. Currently efforts are underway to quantify the forces acting on the indenter such that we may be able to compare our model on a 1:1 basis with current atomic force microscopy experiments. Currently the error in experimental measurement of these forces lacks fine resolution. Our procedures and potential appear to be quite accurate for most situations and this will offer us a powerful tool to probe many systems. This quantification can then be compared with local atomic forces, energies, and stresses for a complete descriptive picture of the material.

Reference List

1. Campbell,S.A. The Science and Engineering of Microelectronic Fabrication. Oxford University Press, Oxford (2001).

2. Kondo,Y., Ru,Q. & Takayanagi,K. Thickness induced structural phase transition of gold nanofilm. *Physical Review Letters* **82**, 751-754 (1999).

3. Kondo,Y. & Takayanagi,K. Gold nanobridge stabilized by surface structure. *Physical Review Letters* **79**, 3455-3458 (1997).

4. Diao,J.K., Gall,K. & Dunn,M.L. Surface stress driven reorientation of gold nanowires. *Physical Review B* **70**, (2004).

5. Diao,J.K., Gall,K. & Dunn,M.L. Surface-stress-induced phase transformation in metal nanowires. *Nature Materials* **2**, 656-660 (2003).

6. Kondo,Y. & Takayanagi,K. Synthesis and characterization of helical multi-shell gold nanowires. *Science* **289**, 606-608 (2000).

7. Tosatti,E., Prestipino,S., Kostlmeier,S., Dal Corso,A. & Di Tolla,F.D. String tension and stability of magic tip-suspended nanowires. *Science* **291**, 288-290 (2001).

8. Tosatti,E. & Prestipino,S. Materials science - Weird gold nanowires. *Science* **289**, 561-563 (2000).

9. Ju,S.P., Lin,J.S. & Lee,W.J. A molecular dynamics study of the tensile behaviour of ultrathin gold nanowires. *Nanotechnology* **15**, 1221-1225 (2004).

10. Hasmy,A., Serena,P.A. & Medina,E. Molecular dynamics simulations for metallic nanosystems. *Molecular Simulation* **29**, 427-435 (2003).

11. Gulseren,O., Ercolessi,F. & Tosatti,E. Noncrystalline structures of ultrathin unsupported nanowires. *Physical Review Letters* **80**, 3775-3778 (1998).

12. Landman,U., Luedtke,W.D., Burnham,N.A. & Colton,R.J. Atomistic Mechanisms and Dynamics of Adhesion, Nanoindentation, and Fracture. *Science* **248**, 454-461 (1990).

13. Untiedt,C., Rubio,G., Vieira,S. & Agrait,N. Fabrication and characterization of metallic nanowires. *Physical Review B* **56**, 2154-2160 (1997).

14. Marszalek,P.E., Greenleaf,W.J., Li,H.B., Oberhauser,A.F. & Fernandez,J.M. Atomic force microscopy captures quantized plastic deformation in gold

nanowires. *Proceedings of the National Academy of Sciences of the United States of America* **97**, 6282-6286 (2000).

15. Agrait,N., Rubio,G. & Vieira,S. Plastic-Deformation of Nanometer-Scale Gold Connective Necks. *Physical Review Letters* **74**, 3995-3998 (1995).

16. Agrait,N., Rubio,G. & Vieira,S. Plastic deformation in nanometer scale contacts. *Langmuir* **12**, 4505-4509 (1996).

17. Pascual,J.I. *et al.* Properties of Metallic Nanowires - from Conductance Quantization to Localization. *Science* **267**, 1793-1795 (1995).

18. Rubio,G., Agrait,N. & Vieira,S. Atomic-sized metallic contacts: Mechanical properties and electronic transport. *Physical Review Letters* **76**, 2302-2305 (1996).

19. Diao,J.K., Gall,K. & Dunn,M.L. Yield strength asymmetry in metal nanowires. *Nano Letters* **4**, 1863-1867 (2004).

20. Frederico,D.N.A., da Silva,E.Z., da Silva,A.J.R. & Fazzio,A. Effect of impurities on the breaking of Au nanowires. *Surface Science* **566**, 367-371 (2004).

21. da Silva,E.Z., da Silva,A.J.R. & Fazzio,A. Breaking of gold nanowires. *Computational Materials Science* **30**, 73-76 (2004).

22. da Silva,E.Z., Novaes,F.D., da Silva,A.J.R. & Fazzio,A. Theoretical study of the formation, evolution, and breaking of gold nanowires. *Physical Review B* **69**, (2004).

23. Novaes,F.D., da Silva,A.J.R., da Silva,E.Z. & Fazzio,A. Effect of impurities in the large Au-Au distances in gold nanowires. *Physical Review Letters* **90**, (2003).

24. da Silva,E.Z., da Silva,A.J.R. & Fazzio,A. How do gold nanowires break? *Physical Review Letters* **87**, (2001).

25. Coura,P.Z. *et al.* On the structural and stability features of linear atomic suspended chains formed from gold nanowires stretching. *Nano Letters* **4**, 1187-1191 (2004).

26. Koizumi,H., Oshima,Y., Kondo,Y. & Takayanagi,K. Quantitative high-resolution microscopy on a suspended chain of gold atoms. *Ultramicroscopy* **88**, 17-24 (2001).

27. Tian,M.L., Wang,J.U., Kurtz,J., Mallouk,T.E. & Chan,M.H.W. Electrochemical growth of single-crystal metal nanowires via a two-dimensional nucleation and growth mechanism. *Nano Letters* **3**, 919-923 (2003).

28. Xiao,Z.L. *et al.* Fabrication of alumina nanotubes and nanowires by etching porous alumina membranes. *Nano Letters* **2**, 1293-1297 (2002).

29. Martin,C.R. Nanomaterials - A Membrane-Based Synthetic Approach. *Science* **266**, 1961-1966 (1994).

30. Goring,P. *et al.* Gold/carbon composite tubes and gold nanowires by impregnating templates with hydrogen tetrachloroaurate/acetone solutions. *Nano Letters* **4**, 1121-1125 (2004).

31. Wang,J.G., Tian,M.L., Mallouk,T.E. & Chan,M.H.W. Microtwinning in template-synthesized single-crystal metal nanowires. *Journal of Physical Chemistry B* **108**, 841-845 (2004).

32. <110> symmetric tilt grain-boundary structures in fcc metals with low stacking-fault energies.

33. Gall,K., Diao,J.K. & Dunn,M.L. The strength of gold nanowires. *Nano Letters* **4**, 2431-2436 (2004).

34. Plimpton,S. Fast Parallel Algorithms for Short-Range Molecular-Dynamics. *Journal of Computational Physics* **117**, 1-19 (1995).

35. Daw,M.S. & Baskes,M.I. Embedded Atom Method: Derivation and application to impurities, surfaces, and other defects in metals. *Physical Review B* **29**, 6443-6453 (84 A.D.).

36. Hohenber H & Kohn W. *Physical Review* **136**, 13864 (1964).

37. Foiles,S.M., Baskes,M.I. & Daw,M.S. Embedded-Atom-Method Functions for the Fcc Metals Cu, Ag, Au, Ni, Pd, Pt, and Their Alloys. *Physical Review B* **33**, 7983-7991 (1986).

38. Plimpton,S.J. & Hendrickson B.A. Parallel Molecular Dynamics With the Embedded Atom Method. Broughton J. and Bristowe P. 37. 1993. Pittsburgh PA, MRS Proceeding 291. Materials Theory and Modelling.

Ref Type: Conference Proceeding

39. Nose,S. & Klein,M.L. Constant Pressure Molecular-Dynamics for Molecular-Systems. *Molecular Physics* **50**, 1055-1076 (1983).

40. Hoover,W.G. Canonical Dynamics - Equilibrium Phase-Space Distributions. *Physical Review A* **31**, 1695-1697 (1985).

41. Ikeda,H. *et al.* Strain rate induced amorphization in metallic nanowires. *Physical Review Letters* **82**, 2900-2903 (1999).

42. Liang,W. & Zhou,M. Response of copper nanowires in dynamic tensile deformation. *Proceedings of the Institution of Mechanical Engineers Part C-Journal of Mechanical Engineering Science* **218**, 599-606 (2004).

43. Egami,T., Maeda,K. & Vitek,V. Structural Defects in Amorphous Solids - A Computer-Simulation Study. *Philosophical Magazine A-Physics of Condensed Matter Structure Defects and Mechanical Properties* **41**, 883-901 (1980).

44. Cheung,K.S. & Yip,S. Atomic-Level Stress in An Inhomogeneous System. *Journal of Applied Physics* **70**, 5688-5690 (1991).

45. Diao,J.K., Gall,K. & Dunn,M.L. Atomistic simulation of the structure and elastic properties of gold nanowires. *Journal of the Mechanics and Physics of Solids* **52**, 1935-1962 (2004).

46. Meyers M A. & Chawla K.K. Mechanical Behavior of Materials. Princeton-Hall, New Jersey (1998).

47. Kelchner,C.L., Plimpton,S.J. & Hamilton,J.C. Dislocation nucleation and defect structure during surface indentation. *Physical Review B* **58**, 11085-11088 (1998).

48. Tian,M.L., Wang,J.U., Kurtz,J., Mallouk,T.E. & Chan,M.H.W. Electrochemical growth of single-crystal metal nanowires via a two-dimensional nucleation and growth mechanism. *Nano Letters* **3**, 919-923 (2003).

49. Wu,B., Heidelberg,A. & Boland,J.J. Mechanical properties of ultrahigh-strength gold nanowires. *Nature Materials* **4**, 525-529 (2005).

(6) Listing of all publications and technical reports supported under this grant or contract. Provide the list with the following breakout, and in standard format showing authors, title, journal, issue, and date.

(a) Papers published in peer-reviewed journals:
Hyde B, Espinosa H D, Farkas D. An atomistic investigation of the elastic and plastic properties of Au nanowires. *JOM* **57** (9) 62-66 (2005)

(b) Papers published in non-peer-reviewed journals or in conference proceedings
No papers were published in non-peer-reviewed journals or conference proceedings

(c) Papers presented at meetings, but not published in conference proceedings
No papers were presented at meetings, but not published in conference proceedings

(d) Manuscripts submitted, but not published
No manuscripts were submitted, but not published

(e) Technical reports submitted to ARO
Technical Report on Atomistic and Dislocation Dynamic Modeling of Plasticity in Polycrystalline Metals

(7) List of all participating scientific personnel showing any advanced degrees earned by them while employed on the project

Brian Hyde – Post Doctoral Researcher
Horacio Espinosa – Principle Investigator
Ravi Agrawal – Graduate Student

(8) Report of Inventions (by title only)
No inventions resulted.

(9) Bibliography
Available in the extended Technical Report

(10) Appendixes
No appendixes are attached to this document